Available online at www.sciencedirect.com

ScienceDirect

Procedia Structural Integrity 2 (2016) 3515–3522

Structural Integrity Procedia

www.elsevier.com/locate/procedia

21st European Conference on Fracture, ECF21, 20-24 June 2016, Catania, Italy

Short and long crack growth behavior of welded ferritic stainless steel

Manon Abecassis[a]*, Alain Köster[a], Vincent Maurel[a]

[a]*MINES ParisTech, PSL Research University, MAT - Centre des matériaux, CNRS UMR 7633, BP 87 91003 Evry, France*

Abstract

To analyze the influence of welding on fatigue crack growth, several geometrical configurations have been tested using notched specimens with notch located within base metal and welded joint. This methodology has shown that fatigue crack growth rate was similar for base metal and welded part for the ferritic stainless steel F18TNb (corresponding to AISI 441 or EN 1.4509 grades) considering long crack. Whereas for short crack, the microstructure induced by the welding process was evidenced to drastically increase the resulting crack growth rate. The tested configurations have been systematically modeled by finite element analysis to obtain reliable shape function and SIF assessment for the chosen geometries. Then fatigue crack growth behavior is discussed on the basis of both SIF values and the influence of microstructure in crack path and crack growth rate.

Keywords: Ferritic stainless steel ; weldment ; crack growth modelling ; grain size gradient

1. Introduction

Ferritic stainless steels are usually used in automotive industry and often assembled by welding. Welding is well known to modify locally the microstructure as compared to the base metal (Tsukamoto, Harada, and Bhadeshia 1994; Zambon and Bonollo 1994). The welded joint consists of the base metal, the fusion zone separated by a transition area from the base metal, the so-called heat affected zone. These areas have different microstructures but also exhibit dissimilar mechanical behaviors from the base metal to the welded joint (Fu and Shi 1996).

Considering fatigue crack growth in the presence of welded parts, it has been established that the microstructure of the welded joint has an impact on the crack path (Ritchie 1988). The crack in the welded joint could deflect to the base metal for dissimilar steel welded joint (H. T. Wang 2013) or otherwise the crack could be straight in the welded joint and become tortuous in the base metal (Trudel, Lévesque, and Brochu 2014). Some branching and deflection were also observed for Q345 steel (Xiong and Hu 2012).

As a direct consequence of the fatigue crack interaction with the microstructure inherited from the welding process, for HT80 welded steel (Ohta et al. 1982) and for 444 welded stainless steel (Akita et al. 2006), fatigue crack growth rate was observed to be different in the threshold region but to be similar in the Paris region comparing base metal and fusion zone. This point is consistent with the influence of the grain size on fatigue crack growth evidenced by (Kusko, Dupont, and Marder 2004) for a 316L austenitic stainless steel: small grain size involves lower fatigue crack growth rate than large grain size in the threshold region, whereas no significant difference was observed for fatigue crack growth rate in the Paris region for all tested different

* Corresponding author.
E-mail address: manon.abecassis@mines-paristech.fr

10.1016/j.prostr.2016.06.438

grain size. (Vasudevan, Sadananda, and Rajan 1997) studied the effect of grain size on the stress intensity factor and crack path of long cracks: grain size, precipitate spacing and slip mode were shown to influence both the crack path and the crack closure effect.

The aim of this study was to analyze the effect of the welded joint on the fatigue crack growth rate and the crack path for a welded F18TNb ferritic stainless steel.

2. Material

2.1. Material description

The material used in this study is the ferritic stainless steel F18TNb (corresponding to AISI 441 or EN 1.4509 grades). Its chemical composition is detailed in Table 1.

Table 1 - Chemical compounds of the studied ferritic stainless steel (at weight) (Bucher 2004)

C	N	Cr	Ti	Nb	Si	Mn	Fe
0.017	0.02	17.67	0.15	0.5	0.59	0.42	Bal.

The butt-welded joint is built from two 2 mm-thick plates using an arc welding procedure. The plates were welded by metal inert gas (MIG) using 1.4511 steel as filler metal. Welded specimens are extracted from the welded plate, the weld bead being located at the center of the specimen.

The microstructure is revealed by an electrolytic etching technique with a nitric acid solution (50% H_2O, 50% HNO_3). Three main areas could be distinguished Figure 1(b):

- Columnar grains area, called the “fusion zone” (FZ). After the melting of the metal due to the welded process, grains become columnar from the butt metal to the center of the weld joint during recrystallization.
- Small equiaxed grains far from the fusion zone. It is the initial microstructure called “Base metal” (BM).
- Transition zone between the base metal and the fusion zone: the “heat affected zone” (HAZ). This area is annealed by heat diffusion.

Table 2 - Grain size in the base metal

	Rolling direction (RD)	Transverse direction (TD)	Normal direction (ND)
Base metal	40-43 µm	41-45 µm	50-51 µm

In the base metal, grains were observed to be equiaxed in all directions, with a size ranging from 40 to 50 µm (Figure 1(a) and Table 2). The fusion zone is made of columnar grains with an average length of 800 µm and a width of 200 µm.

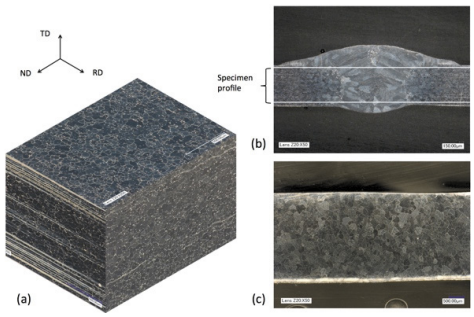

Figure 1 - Grain size structure gradient: (a) base metal in all directions, (b) side view of the specimen (RD-TD) plane and (c) fusion zone (TD-ND) plane

2.2. Specimen geometry

Center Cracked Tension (CCT) specimens were used to analyze crack growth. First the weld was machined to obtain a uniform section of 2 mm in thickness. The Figure 1(b) shows the initial profile of the welded zone where the final specimen section is highlighted using white lines. Then, the CCT specimens were processed by Electro Discharge Machining (EDM) from welded plates (Figure 2). A single notch was machined at the center of the specimen (and at the center of the weld) with a width of 1.6 mm as shown in Figure 2. Finally, the specimen faces were polished up to 1200 SiC paper, and then with 3 µm and 1 µm diamond polishing paste.

Three kind of specimens were studied:

- Base metal specimen, where the notch was orthogonal to the loading direction; Figure 2(b).
- Welded specimen, named N90-welded, where both the welded joint and the notch were orthogonal to the loading direction; Figure 2(b).
- Oriented welded specimen, named N60-welded, where both the welded joint and the notch were tilted to form a 60° angle to the loading direction; Figure2(c).

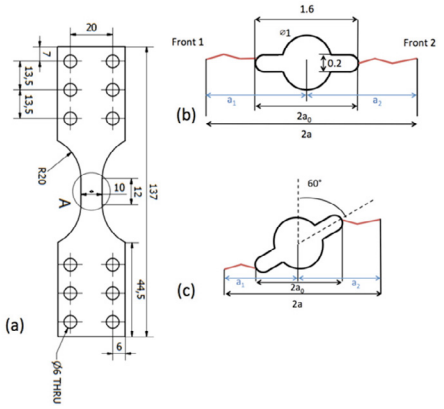

Figure 2 –Specimen and notch geometries: (a) specimen, (b) notch for base metal and N90-welded specimen, (c) notch for N60-welded specimen

3. Experimental procedure

Fatigue crack growth tests have been carried out at room temperature using a hydraulic fatigue machine. The tests were stress controlled using a loading with sinusoidal wave, the stress amplitude was of constant amplitude and the load ratio was set to R_σ=0.1. The test conditions are summarized in Table 3. The crack length was optically measured on each side of the notch from the notch center to the crack tip projected orthogonally to the loading direction (a_1, crack length of front 1 and a_2, crack length of front 2 as shown in Figure2(b)). The crack length a results of the averaging of a_1 and a_2 length.

A pre-crack stage has been applied up to a crack length extension of about 100 µm for each specimen. Considering the notch geometry, the pre-crack was equivalent to a_0=0.8 mm for the base metal and the N90-welded specimens and to a_0=0.5 mm for the N60-welded specimen respectively.

Table 3 - Test conditions: P corresponds to the applied load, Δσ is the nominal stress amplitude, a_0 and a_f are the initial and final crack length respectively and ΔK_{init} and ΔK_{final} are the initial and final SIF amplitude respectively

Specimen	Notch orientation (and weld orientation)	P_{max} (kN)	P_{min} (kN)	Δσ (MPa)	a_0 (mm)	a_f (mm)	ΔK_{init} (MPa. $m^{1/2}$)	ΔK_{final} (MPa. $m^{1/2}$)
Base metal	90°	3.0	0.3	150	0.861	2.897	6.9	17.3
N90-Welded	90°	3.0	0.3	150	0.851	2.777	6.9	16.5
N60-Welded	60°	4.0	0.4	200	0.506	1.753	5.1	14.7

In the test, crack growth length was measured by direct current potential drop (DCPD) technique (Clark and Knott 1975; Hartman and Johnson 1987; Doremus et al. 2015). Two probes were fixed using micro-welding method at a distance of 1 mm from the initial center of the notch, one probe below and one probe above the notch considering the loading direction. A Keyence VHX1000 microscope was used to measure *in situ* the surface crack length. During the test, both the potential drop and the crack images have been stored. These images were then used for optical calibration of DCPD. The potential versus crack growth curve has been approximated by two-degrees polynomial curve as the calibration curve.

To obtain reliable fatigue crack growth rate measurement, the ratio of a constant increment of crack length Δa of 50 µm by the corresponding increment of number of cycle ΔN yields $da/dN \approx \Delta a/\Delta N$. Moreover, the amplitude of the stress intensity factor ΔK was calculated using:

$$\Delta K = Y\left(\frac{a}{b}\right) * \Delta\sigma * \sqrt{\pi a}$$

with Y the shape (or correction) function, a the crack length, $\Delta\sigma$ the stress and b the specimen half-width. Because the design of the specimens was non-standard, the shape functions of the specimen geometry were derived from Finite Element Analysis (FEA) as detailed in the next section.

4. Modeling

To obtain the shape function irrespectively of the tested configuration (*i.e.* irrespectively of the notch angle to the loading direction), a Finite Element Analysis of the crack growth was performed using conform remeshing techniques included in the Z-set software (Zset software; Missoum-benziame et al. 2011). The specimens have been modeled with 3D linear tetrahedron as shown in Figure 3 (b) and (c). The mesh was refined in the vicinity of the crack front with a minimum mesh size of 25 µm. The crack path was approximated as a straight-path orthogonal to the loading direction. The crack growth analysis was achieved from an initial penny shape crack corresponding to a crack extension of 0.10 µm up to a crack extension of 1.6 mm. The shape function was deduced from stress intensity factor that was derived on the basis of J integral and interaction integral techniques (Chiaruttini et al. 2012). As a first assumption only mode I has been considered in the present study.

An abacus (Tada, Paris, and Irwin 1973) exists for crack emanating from a circular hole through an infinite medium (see Figure 3(a)). The specimens used in our study differ from the geometry reference: they were of finite uniform thickness with differences also in notch shape (see Figure 3). The shape function depends of two main geometrical parameters:

- The R/b ratio is used to describe the notch radius R and specimen half-width b
- The h/b ratio is used to describe the gauge length h and specimen half-width b.

The specimen geometry used in this study is of uniform thickness where h/b=1.2 for a more complex notch shape that was found in the abacus. Nevertheless, two geometries from the abacus could give approximation of the tested configuration: a 1 mm diameter hole (R/b=0.1) and a 1.6 mm diameter hole (R/b=0.16) respectively. Therefore, these two configurations have been modeled by FEA to test the reliability of the chosen method. This constitutes a basic comparison with the abacus, using a major bound with an equivalent circular diameter of 1.6 mm, which is the length of the real notch, and a minor bound with an equivalent circular diameter of 1 mm, corresponding to the actual circular hole present in the notch. Indeed, for this latest geometry when the crack reaches a/b=0.16, it was corresponding to the real notch length.

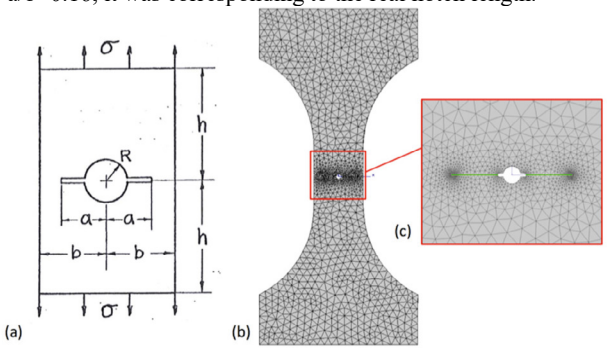

Figure 3 – (a) Abacus' geometry of the specimen (Tada, Paris, and Irwin 1973), (b) specimen model, (c) zoom on the notch and the crack

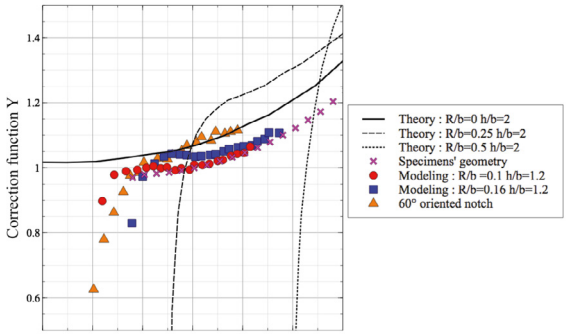

Figure 4 - Correction functions from the abacus of (Tada, Paris, and Irwin 1973), lines, and for FE analysis of two geometries of the specimen (oriented and non-oriented notches), symbols.

For h/b=2 and b set to a constant value, three curves have been extracted from the abacus, corresponding to no-hole configuration (R/b=0), a 2 mm diameter hole (R/b=0.25) and a 5 mm diameter hole (R/b=0.5) respectively (Figure 4). For the three cases of the abacus, and for a constant value of b, the initial value of the ratio a/b is proportional to the ratio R/b. It is

observed for the abacus, that the higher the initial a/b (or R/b) ratio the higher the value of the Y function for large values of a/b ratio, leading to a crossing of Y curves. These trends are consistently observed for Y function derived from the present FEA. Considering the real shape of the notch, the shape function increases from 1 to 1.2 for a/b ratio varying from 0.2 to 0.6. In all cases, the correction function is an amplification function of the stress intensity factor. However for the N60-welded specimen, the notch was of the same geometry as for base metal and N90-welded specimen (pink crosses in Figure 4), but the notch was oriented with a 60° angle to the load direction leading to a significant modification of the correction function (orange triangles in Figure 4).

5. Experimental results

5.1. Crack path

For the base metal, the crack path was mostly orthogonal to the loading direction and rather straight for crack extension lower than 1.1 mm (Figure 5(a)). For longer crack length, a deflection of about 15° was measured as the angle formed between crack path and the direction orthogonal to the loading direction. The N60-welded specimen has shown global bifurcation of about 24° for the left side and 15° for the right side, even for short crack (Figure 5(c)).

For both welded specimens (N90- and N60-welded), local bifurcations were systematically observed and more pronounced than for the base metal: deflection angles between 36° and 90° were measured (Figure 5(b) et (c)). At a more local scale (see Figure 6), crack branching has been observed. Moreover, the length of the straight crack path in the welded joint is longer (about 180 µm) than in the base metal (30 µm length). It is worth noting that these lengths are very closed to the measured grain size.

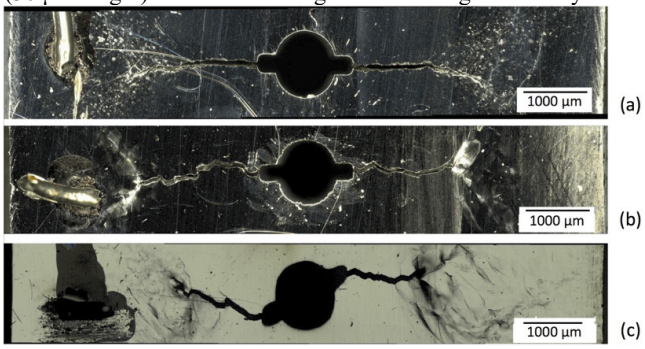

Figure 5 - Crack paths observed at the end of the test for (a) Base metal, (b) N90-Welded and (c) N60-Welded specimens. (observations were made with a 0.1kN applied loading)

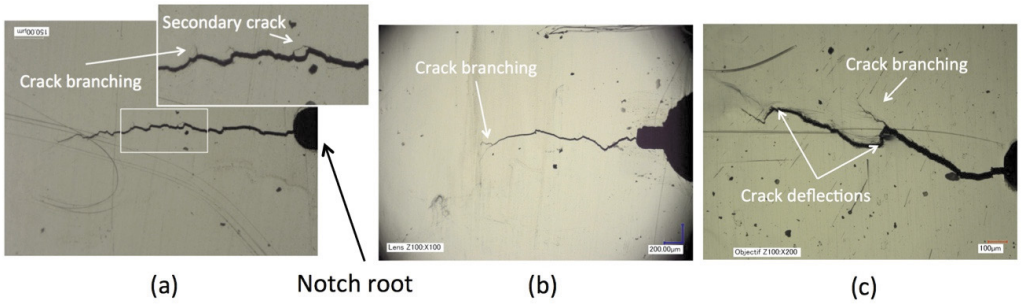

Figure 6 – Partial view of crack branching, crack deflection and secondary crack for (a) base metal, (b) N90-Welded and (c) N60-Welded specimens (observations were made with a 0.1kN applied loading)

5.2. Observation of grains and crack paths

The Electron Backscatter Diffraction (EBSD) method was used to determine the position of the crack paths related to the microstructure (Figure 7). It was not possible to determine the transgranular or intergranular crack propagation for the base metal specimen since the grain size was too small as compared to crack opening and subsequent rotation of grains (Figure 7(a)). But, in the N90- and N60-welded specimen, the propagation was observed to be mostly transgranular (Figure 7(b) and (c)).

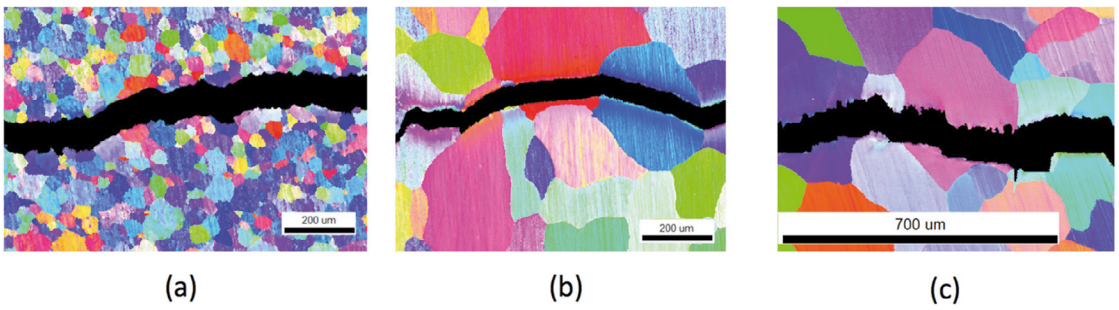

Figure 7 - Grains were highlighted using EBSD. The crack paths correspond to the major crack growing from the right to the left side of the pictures for (a) Base metal, (b) N90-Welded and (c) N60-Welded specimens

5.3. Fatigue crack propagation

Figure 8 shows plots of crack length versus number of cycles rationalized by the maximum number of cycles. The crack growth in the base metal has initiated more slowly as compared to the two welded specimens. The most detrimental condition was observed for N60-welded specimen, when considering the number of cycles to reach a given crack length.

The crack growth rate derived from crack length was then plot as a function of the stress intensity factor amplitude ΔK derived from FEA as described above (Figure 9). For the three specimens, near-threshold region has been evidenced at low value of stress intensity factor, without reaching actual threshold. In the Paris Law regime, the crack propagation rates were observed to be similar for both base metal and N90-welded specimens (Figure 9(a)). Nevertheless, for the N90-welded curve, local growth rate jumps can be observed that are certainly due to the local deflections associated to large grain size as discussed above for relatively short crack (Figure 9(b)). Nevertheless, Paris law was identified for each tested configuration, using:

$$\frac{da}{dN} = C\,\Delta K^m$$

where C and m are Paris' Law parameters. An exponent m=4 was observed to fit all tests considering long crack range; the coefficients C are very close to each other for both base metal and N90-welded specimens.

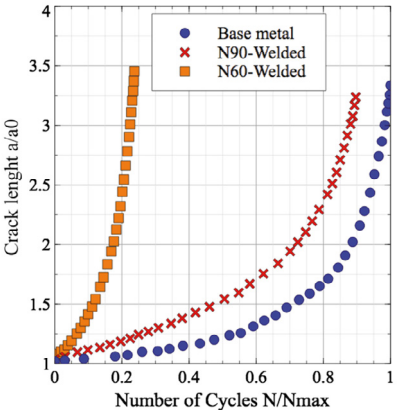

Figure 8 - Evolution of the crack length a/a_0 in function of the number of cycle N/N_f for base metal and welded specimens

For the N60-welded specimen, a slope modification has been observed for ΔK~8 MPa.$m^{0.5}$. For long crack, the exponent m=4 fit experimental results very well, whereas for short cracks m=2. The effect of short crack was more pronounced with the N60-welded geometry than in the N90-welded geometry: the crack growth rate was faster in the N60-welded specimen even if the slope was lower than in N90-welded specimen.

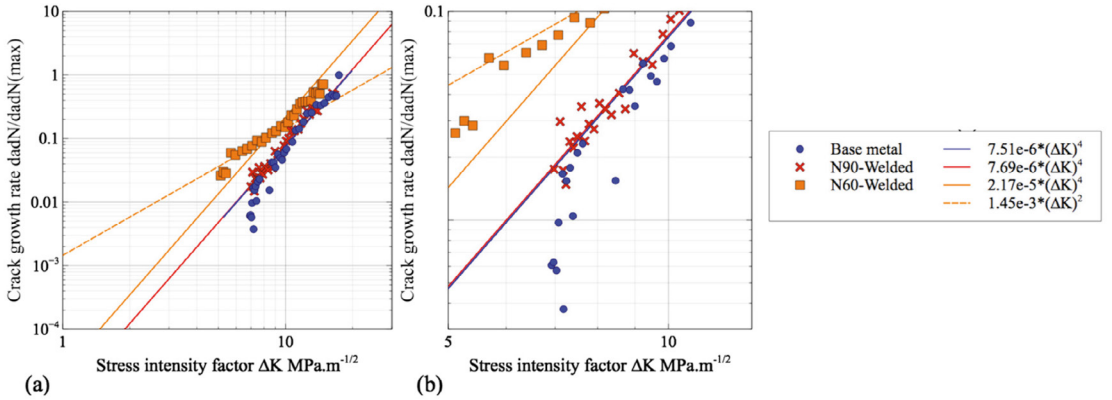

Figure 9 - Fatigue crack propagation for base metal and welded specimens (a) general view (b) zoom

6. Conclusion and discussion

This study has promoted a full analysis of interaction between fatigue crack growth and microstructure for ferritic welded stainless steel. A CCT specimen was designed using orthogonal or non-orthogonal notch to the loading direction. Together with this design, shape functions were obtained for each tested configuration on the basis of finite element analysis. Thus crack growth rate could be derived from crack length measurement and modeled SIF amplitude. In the Paris region, the crack growth properties of the base metal and N90-welded are close to each other. Moreover, for long crack, the crack growth rate slope was the same for any tested configuration. These results are fully consistent with crack growth tests achieved with a 444 ferritic stainless steel which has a very closed chemical composition to the base metal (Akita et al. 2006). In this study authors have shown that the crack propagation rate are similar in the Paris region but different in the threshold region.

However, our study has clearly evidenced that at low ΔK values, the crack growth rates were faster in the welded joint (N90- and N60-welded) than in the base metal with a very critical configuration associated to the N60-welded specimen where crack path was not confined to the center of the welded joint. Thus this configuration was seen to stress out the short crack to crystallographic texture interaction. Finally, even if crack growth slope was the same for long crack, this last configuration has led to a rough increase of the crack growth rate for any crack length. It is worth noting that the present analysis did not include actual crack path. Particularly, an in-depth analysis of the N60-welded test configuration is underway. In this case mixity of mode I and II is modifying the effective crack growth rate that should be accounted for.

Acknowledgements

The authors thank Pierre-Oivier Santacreu APERAM for providing the base and the welded material. Dr. Vladimir Esin is gratefully acknowledged for the assistance with EBSD experiments.

References

Masayuki, A., Nakajima, M., Tokaji, K., Shimizu, T., 2006. Fatigue Crack Propagation of 444 Stainless Steel Welded Joints in Air and in 3%NaCl Aqueous Solution. Materials & Design 27 (2), 92–99.

Bucher, L., 2004. Etude de l'endommagement en fatigue thermique des aciers inoxydables F17TNb et R20-12 pour application automobile. PhD thesis, École Nationale Supérieure des Mines de Paris. https://pastel.archives-ouvertes.fr/tel-00163013/document.

Chiaruttini, V., Geoffroy, D., Riolo, V., Bonnet, M., 2012. An Adaptive Algorithm for Cohesive Zone Model and Arbitrary Crack Propagation. Revue Européenne de Mécanique Numérique/European Journal of Computational Mechanics 21,: 208–18.

Clark, G, Knott, J., 1975. Measurement of Fatigue Cracks in Notched Specimens by Means of Theoretical Electrical Potential Calibrations. Journal of The Mechanics and Physics of Solids 23, 265–76.

Doremus, L., Nadot, Y., Henaff, G., Mary, C., Pierret, S., 2015. Calibration of the Potential Drop Method for Monitoring Small Crack Growth from Surface Anomalies – Crack Front Marking Technique and Finite Element Simulations. International Journal of Fatigue 70, 178–85.

Fu, J. Q., Shi, Y. W., 1996. Effect of Cracked Weld Joint and Yield Strength Dissimilarity on Crack Tip Stress Triaxiality. Theoretical and Applied Fracture Mechanics 25 (1), 51–57.

Hartman, G. A., Johnson, D. A., 1987. D-c Electric-Potential Method Applied to Thermal/mechanical Fatigue Crack Growth. Experimental Mechanics 27 (1), 106–12.

Wang, H. T., Wang, G. Z., 2013. An Experimental Investigation of Local Fracture Resistance and Crack Growth Paths in a Dissimilar Metal Welded Joint. Materials & Design 44, 179–89.

Kusko, C. S., Dupont, J. N., Marder, A. R., 2004. The Influence of Microstructure on Fatigue Crack Propagation Behavior of Stainless Steel Welds. Welding Journal 83 (1), 6–14.

Missoum-benziame, D., Chiaruttini, V., Garaud, J.-D., Feyel, F., Foerch, R., Osipov, N., Quilici, S., Rannou, J., Roos, A., Ryckelynck, D., 2011. Z-set/ZeBuLoN : Une Suite Logicielle Pour La Mécanique Des Matériaux et Le Calcul de Structures, 10e colloque national en calcul des structures, 8.

Ohta, A., Sasaki, E., Nihei, M., Kosuge, M., Kanao, M., Inagaki, M., 1982. Fatigue Crack Propagation Rates and Threshold Stress Intensity Factors for Welded Joints of HT80 Steel at Several Stress Ratios. International Journal of Fatigue 4 (4), 233–37.

Ritchie, R. O. 1988. Mechanisms of Fatigue Crack Propagation in Metals, Ceramics and Composites: Role of Crack Tip Shielding. Materials Science and Engineering: A 103 (1), 15–28.

Tada, H., Paris, P.C., Irwin, G. R., 1973. The Stress Analysis of Cracks Handbook. Three Park Avenue New York, NY 10016-5990: ASME.

Trudel, A., Lévesque, M., Brochu, M., 2014. Microstructural Effects on the Fatigue Crack Growth Resistance of a Stainless Steel CA6NM Weld. Engineering Fracture Mechanics 115, 60–72.

Tsukamoto, S., Harada, H., Bhadeshia, H. K. D. H., 1994. Metastable Phase Solidification in Electron Beam Welding of Dissimilar Stainless Steels. Materials Science and Engineering: A 178 (1), 189–94.

Vasudevan, A. K, Sadananda, K., Rajan, K., 1997. Role of Microstructures on the Growth of Long Fatigue Cracks. International Journal of Fatigue, 19 (93), 151–59.

Xiong, Y., Hu, X. X., 2012. The Effect of Microstructures on Fatigue Crack Growth in Q345 Steel Welded Joint. Fatigue & Fracture of Engineering Materials & Structures 35 (6), 500–512

Zambon, A., Bonollo, F., 1994. Rapid Solidification in Laser Welding of Stainless Steels. Materials Science and Engineering A 178 (1), 203–7.

Zset software. n.d. Non-Linear Material & Structure Analysis Suite. http://www.zset-software.com.